3

Postembedding Immunogold Cytochemistry of Membrane Molecules and Amino Acid Transmitters in the Central Nervous System

THOMAS MISJE MATHIISEN, ERLEND ARNULF NAGELHUS, BAHAREH JOULEH, REIDUN TORP, DIDRIK SØLIE FRYDENLUND, MARIA-NIKI MYLONAKOU, MAHMOOD AMIRY-MOGHADDAM, LUCIENE COVOLAN, JO KRISTIAN UTVIK, BJØRG RIBER, KAREN MARIE GUJORD, JORUNN KNUTSEN, ØIVIND SKARE, PETTER LAAKE, SVEND DAVANGER, FINN-MOGENS HAUG, ERIC RINVIK, and OLE PETTER OTTERSEN

THOMAS MISJE MATHIISEN, ERLEND ARNULF NAGELHUS, BAHAREH JOULEH, REIDUN TORP, DIDRIK SØLIE FRYDENLUND, MARIA-NIKI MYLONAKOU, MAHMOOD AMIRY-MOGHADDAM, LUCIENE COVOLAN, JO KRISTIAN UTVIK, BJØRG RIBER, KAREN MARIE GUJORD, JORUNN KNUTSEN, ØYVIND SKARE, PETTER LAAKE, SVEND DAVANGER, FINN-MOGENS HAUG, ERIC RINVIK, AND OLE PETTER OTTERSEN • Centre for Molecular Biology and Neuroscience, and Nordic Centre for Research on Water Imbalance Related Disorders (WIRED), Institute of Basic Medical Sciences, University of Oslo, PO Box 1105 Blindern, N-0317 Oslo, Norway

Abstract: This chapter deals with procedures for postembedding labeling of brain sections embedded in epoxy or methacrylate resins and focuses on protocols that are based on freeze substitution of chemically fixed tissue. When optimized for the target epitope, such protocols offer a high labeling efficiency and allow simultaneous visualization of several antigens by use of different-sized gold particles. Postembedding labeling can be combined with anterograde tracing, permitting the identification of transmitter and postsynaptic receptors of identified axons. By use of tailor-made model systems, antibody selectivity can be monitored in a quantitative manner and under conditions that are representative of the immunocytochemical procedure. Such model systems also allow the generation of calibration curves for assessment of the cellular and subcellular concentration of soluble antigens. When used in conjunction with computer programs for automated acquisition and analysis of gold particles, the postembedding immunogold procedure provides an accurate representation of the cellular and subcellular distribution of proteins and small compounds such as transmitter amino acids. The present chapter provides a quantitative analysis and critical discussion of how changes in incubation parameters influence the labeling intensity. Postembedding immunogold cytochemistry stands out as a powerful technique for analysis of the chemical architecture of the central nervous system and has proved useful for investigating disease processes at the molecular level.

Keywords: aquaporins, glutamate, glutamate receptors, quantitation, resolution, specificity testing

I. INTRODUCTION

The ultimate goal in immunocytochemistry is to be able to determine the exact number and position of a given target molecule in a biological tissue.

A priori, this requires access to monospecific antibodies that bind with a 1:1 stoichiometry to the target antigen, and a reporter system that allows accurate localization and quantitation of the primary antibodies. These are ideal conditions that cannot be met in practice. However, they can be approached by use of markers that are amenable to quantitative electron microscopic analysis.

Colloidal gold particles (Faulk and Taylor, 1971; Roth, 1996; van den Pol, 1989) have proven to be the most versatile markers for this purpose. They are electron dense, allowing easy identification and quantitation in the electron microscope, and can be prepared in many different sizes, permitting simultaneous detection of several different antigens. Most importantly, colloidal gold particles can be coupled directly to the primary or secondary antibody so as to afford a close spatial relation to the target antigen. These features set immunogold cytochemistry apart from the peroxidase–antiperoxidase method and other enzyme-based immunocytochemical techniques. The latter techniques typically rely on the analysis of an electron-dense reaction product that is difficult to quantify and that may diffuse away from the site of formation.

Colloidal gold particles may, in principle, be applied in two different ways: in preembedding or postembedding mode. In the preembedding mode, the antibodies and immunogold reagents are applied to permeabilized tissue that is subsequently embedded in a resin suitable for electron microscopic analysis. In the postembedding mode, the immunoreagents are applied directly onto ultrathin sections of resin-embedded tissue or cells. The latter approach allows immunodetection only of those antigen molecules that are exposed at the surface of the section. This implies that the proportion of antigen molecules that is available for antibody binding is severely restricted when compared with the preembedding mode.

So why use the postembedding mode? The major advantage offered by the postembedding mode is that each antigen molecule that occurs at the surface of the section should stand the same chance of being immunodetected, regardless of its cellular or subcellular localization. This contrasts with the situation in the preembedding mode, where diffusion barriers may constrain the labeling and distort the relationship between antigen concentration and gold particle density. Thus, for the purpose of quantitation, the postembedding procedure is generally considered as the superior of the two modes of immunogold cytochemistry. Preembedding procedures have their own set of advantages that will not be considered here (see Sesack *et al.*, this volume). We also need to emphasize that cryoelectron microscopy is outside the scope of the present chapter, which deals exclusively with postembedding immunogold labeling of resin-embedded sections. The chapter is focused on experience gained in our own laboratory and is not intended to provide a balanced overview of the historical development of the technique. A description of the pioneering work is found elsewhere (Griffiths, 1993; Maunsbach and Afzelius, 1999; Roth, 1996).

II. RESOLUTION

As stated in the Introduction, the resolution of the postembedding immunogold technique exceeds by far the resolution offered by enzyme-based techniques. Thus, with the former technique, the marker is a well-defined particle that is attached to the antigen through an antibody bridge, rather than a reaction product that may be deposited at a distance from its site of formation.

Indeed, it is the length of the antibody bridge and the dimension of the colloidal particle that restrict the resolution of the postembedding immunogold procedure. Theoretically, the distance between the epitope and the center of the gold particle should correspond to the radius of the particle plus the diameters of the interposed immunoglobulins (IgGs) (Fig. 3.1). Using 15-nm gold particles and a primary and secondary IgG (each with an efficient diameter of ~8 nm), this theoretical distance should be ~23 nm. Obviously, the distance will be shorter if colloidal gold is coupled to the primary antibody directly or by way of a secondary Fab complex rather than a secondary IgG.

The theoretical prediction as to lateral resolution is borne out by experiments based on the use of tailor-made model antigens (Fig. 3.2). The model antigens were embedded in the same resin as that used for the tissue, ensuring identical conditions. Further, the antigens were prepared to form discrete bodies with a distinct demarcation from the surrounding resin. Hence, the distance between the margin of the body and the centers

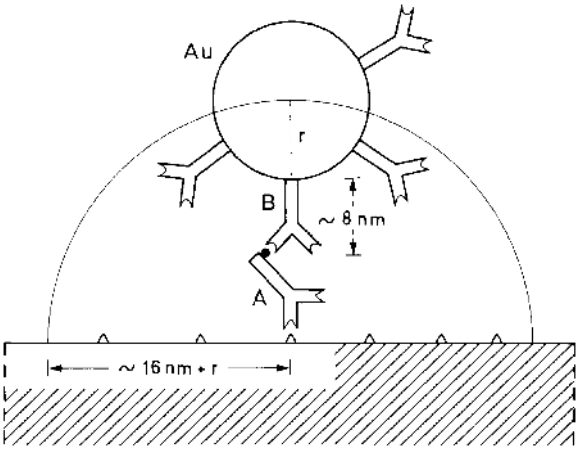

Figure 3.1. Simplified diagram of a two-step, postembedding immunogold procedure. Triangles represent the antigen against which the primary antibody (A) was raised. The secondary antibody (B) is coupled to a colloidal gold particle (Au). The radius (r) of the gold particle is 7.5 nm. This adds up to a maximum distance of about 23 nm between the epitope and the gold particle center (given an effective IgG diameter of 8 nm). (From Ottersen, 1989a.)

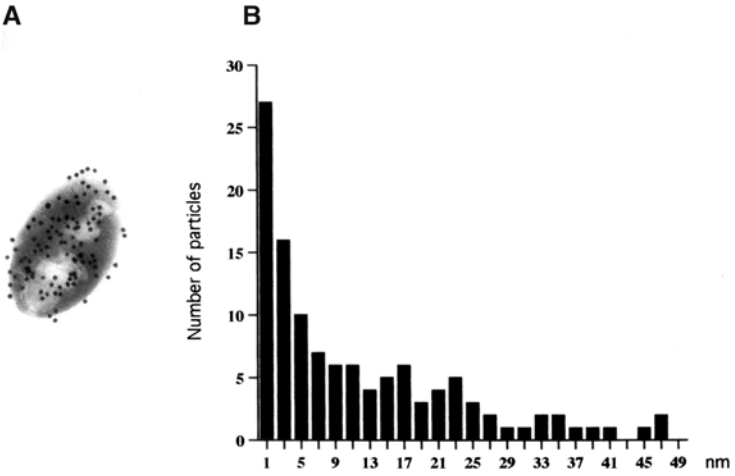

Figure 3.2. Lateral resolution of current immunogold procedure (15-nm gold particles). Values along the *x*-axis in B denote distance from centers of gold particles to the margin of antigen-containing bodies (A). Background level of labeling is reached ~28 nm off the bodies. The data were based on the analysis of 30 bodies containing glutaraldehyde-fixed L-aspartate as a model antigen. Scale bar: 0.3 μm. (From Matsubara *et al.*, 1996.)

of the gold particles should be representative of the lateral resolution of the postembedding immunogold procedure. The gold particle density was found to reach background level at ~28 nm off the margin of the test body (Fig. 3.2B) in good agreement with the theoretical prediction.

Obviously, the above-mentioned theoretically and experimentally determined values represent the *maximum* distance between an epitope and the respective gold particle. In practice, many particles are likely to end up closer to the epitope, due to a restricted rotational freedom. It must also be remembered that the *projected* distance between the gold particle and the epitope may be considerably shorter than the real distance.

This notwithstanding, the fact that the size of the antibody bridge significantly limits the resolution of the postembedding immunogold technique has practical consequences in several experimental settings. Two examples will be used to illustrate this. These examples will also show how the effective resolution can be improved by resorting to tailor-made statistical procedures.

The first example is representative of a common problem in neurobiology: the need to distinguish between two plasma membranes that are closely apposed to one another. A close membrane apposition is typical of central synapses where the pre- and postsynaptic membranes are separated by a synaptic cleft of ~20 nm. This distance is less than the theoretical and experimental maximum values between the epitope and the gold particle center. In other words, a gold particle overlying the presynaptic membrane might reflect antibody binding to an epitope in the postsynaptic membrane,

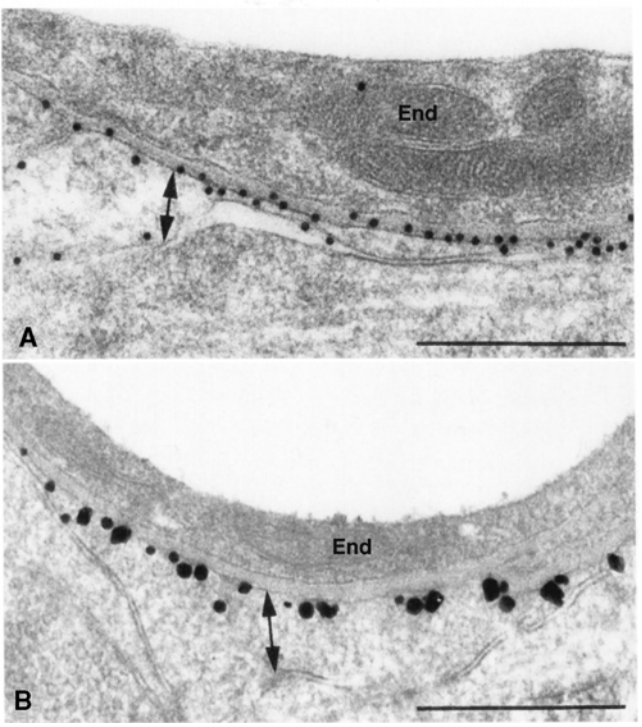

Figure 3.3. Comparison of postembedding (A) and preembedding (B) labeling of AQP4 in perivascular astrocyte end feet membranes (double arrows indicate width of end foot). End, endothelial cell. (A) In the postembedding mode, gold particles are deposited on either side of the membrane—the maximum distance from the membrane reflecting the size of the antibody bridge (cf. Figs. 3.1 and 3.2). (B) In preembedding mode (ultrasmall gold particles enhanced by silver), all particles end up at the cytoplasmic aspect, due to the constraints imposed by the membrane (the epitope is located at the intracellular tail of AQP4). Note variable size and confluence of particles, typical of the preembedding mode. (A, B: From Nielsen *et al.*, 1997.) (C) Analysis of AQP4 immunogold labeling by recording the distribution of gold particles along an axis perpendicular to the labeled plasma membrane (postembedding labeling as in A). The *ordinate* indicates number of gold particles per bin (bin width, 5 nm). The peak coincides with the plasma membrane (0 corresponds to midpoint of membrane) and the particle density approaches background level at ~50 nm from the membrane (inside negative). This section was labeled from both sides, explaining why some particles are located further off than the theoretically and experimentally determined maximum distance between epitope and gold particle (see text). (C: From Nagelhus *et al.*, 1998.)

and vice versa. So how is it possible to determine whether a given antigen is localized pre- and/or postsynaptically?

This question can be resolved by recording the distribution of gold particles along an axis perpendicular to the synaptic membranes (here defined as *z*-axis). Depending, i.a., on the rotational freedom of the epitope and the number of gold particles recorded, the average position of an antigen along this axis can be determined with a precision of ~1 nm,

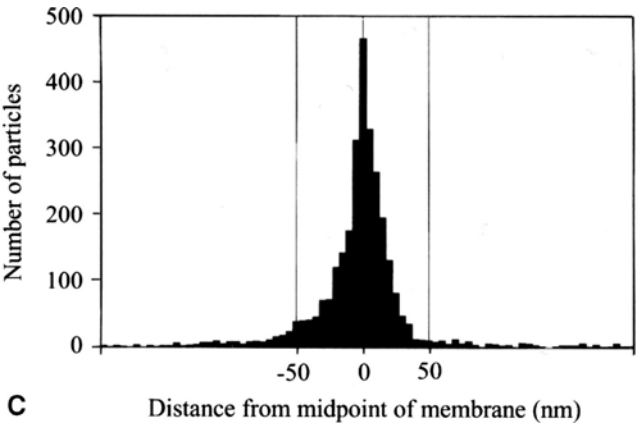

Figure 3.3. (*cont*).

defined by the standard error of the *z*-value of the peak particle density (Fig. 3.3; also see Nagelhus *et al.*, 1998, 2004). By this approach, it was possible to demonstrate that the BK potassium channel is expressed in presynaptic but not in postsynaptic membranes of hippocampal synapses (Hu *et al.*, 2001; Fig. 3.4). The same approach was exploited recently to distinguish between closely apposed membranes in the olfactory bulb (Panzanelli *et al.*, 2004) and has also been used, in a different context, to identify the relative positions of molecules engaged in glutamate receptor complexes (Valtschanoff and Weinberg, 2001). The common practice of labeling both sides of the section may decrease the precision of this approach, as the intersections of a membrane with the two surfaces of the 50- to 100-nm-thick tissue section are rarely superimposed in the image (Fig. 3.5).

The second example of a biological problem that requires due attention to the size of the antibody bridge relates to the analysis of synaptic vesicles (particularly the small, clear vesicles that have a diameter of ~50 nm). The question was whether glutamate is enriched in the synaptic vesicles of granule cell dendritic spines of the olfactory bulb (Didier *et al.*, 2001). These spines are presynaptic to the mitral cell dendrites and display a high density of gold particles signaling glutamate. But this signal could reflect metabolic glutamate, rather than a vesicular pool of transmitter glutamate. Due to the small dimensions of the clear synaptic vesicles, one cannot attach significance to individual gold particles: even a particle located at the center of a vesicle could theoretically depend on an epitope external to the vesicle in question.

To circumvent this problem, measurements were made of the intercenter distances between each gold particle and the nearest synaptic vesicle. It turned out that short distances were overrepresented compared with random distributions of gold particles, supporting the idea that glutamate is associated with synaptic vesicles (Didier *et al.*, 2001).

The two examples discussed above show that statistical analyses of large numbers of gold particles can partly compensate for the inaccuracy

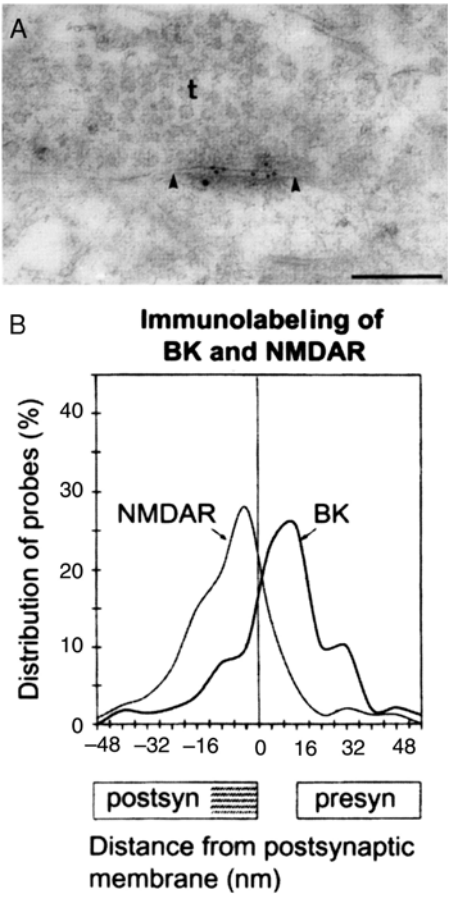

Figure 3.4. Analysis of gold particle distribution in closely apposed synaptic membranes. (A) Electron micrograph showing the distribution of BK channels (10-nm particles) and NMDA receptors (NMDARs; 15-nm particles) in double-labeled sections from the stratum radiatum of CA1. t, terminal; arrowheads indicate extent of postsynaptic density. (B) To determine whether the two epitopes were associated with the pre- and/or postsynaptic membranes, the vertical distribution of particles was analyzed by the approach described in Fig. 3.3. The peak density of particles coincided with the presynaptic membrane in the case of BK channels and with the postsynaptic membrane in the case of NMDARs. The dimensions of the synaptic cleft and postsynaptic density are indicated below the abscissa. (From Hu *et al.*, 2001.)

introduced by the antibody bridge. Other factors that affect the effective resolution of the postembedding technique are discussed in Appendix II. How could resolution be further improved? There is a marginal gain by coupling small gold particles directly to the primary antibodies (or Fab fragments of primary antibodies), rather than to the secondary ones. A substantial increase in resolution would be achieved by visualizing (by negative staining) the antibody bridge between the epitope and the gold particle. But an even larger step toward the "ultimate goal" of defining the precise

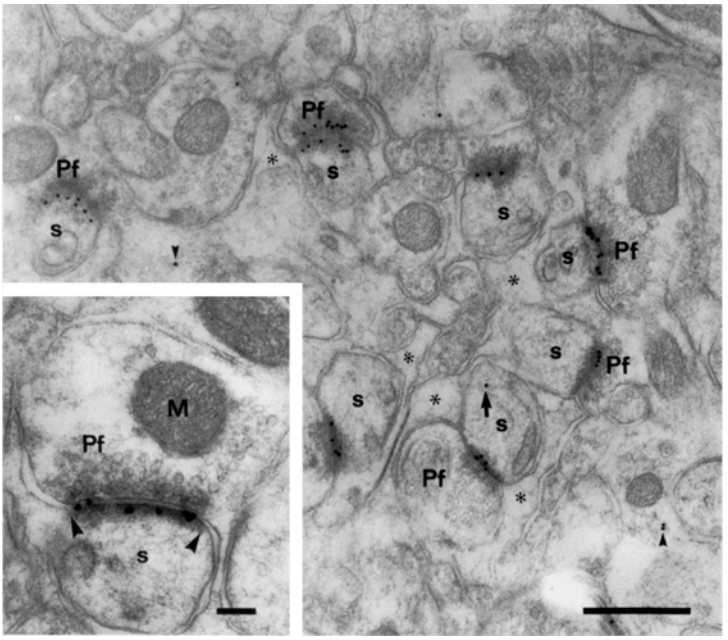

Figure 3.5. Distribution of gold particles signaling δ2-glutamate receptors at synapses between parallel fibers (Pf) and Purkinje cell spines (s) of rat cerebellum. The synapse at top center is obliquely cut, the two rows of particles representing receptors exposed at opposite surfaces of the section (the section was labeled from both sides). Asterisks indicate glial lamellae. The labeling is highly selective: only seven particles in this field are not associated with any postsynaptic density. Of these, one is found within a spine (arrow) and two within other intracellular compartments (arrowheads). The linear density of gold particles (particles per micrometer membrane) in parallel fiber–Purkinje cell synapses was 19.7, compared to 0 in all other types of cerebellar synapse. Inset: Higher magnification of an immunolabeled parallel fiber synapse (postsynaptic density delimited by arrowheads). *M*, mitochondrion. Gold particles, 15 nm. Scale bars: 0.5 μm; 0.1 μm (inset). (From Landsend *et al.*, 1997.)

position of the target antigen is provided by the combination of freeze fracture and immunogold labeling (Fujimoto, 1995; Rash *et al.*, 2004, Hagiwara *et al.*, 2005). With this combination of techniques, the immunogold procedure is employed to determine the molecular identity of intramembrane particles (IMPs) visualized in metal replicas. This approach has proved particularly useful in the case of proteins that are clustered in the plasma membranes, such as connexins and aquaporins. For molecules with a more scattered distribution, the analysis may be hampered by limited sensitivity. This notwithstanding, the freeze fracture–immunogold labeling technique has enormous potential for determining the exact position and number of receptors, transporters, or other molecules in the plasma membranes of neural cells. The extent to which this potential can be realized depends on the ability to classify IMPs according to their sizes and structural features. A

further refinement of the freeze fracture approach is required to define a sufficiently broad range of membrane molecules.

III. QUANTITATION

"Quantitative immunocytochemistry" is considered by many as a contradiction in terms. It is true that we are still far away from the "ultimate goal" of being able to determine the accurate numbers of molecules by means of immunocytochemistry. However, immunogold procedures have brought us closer to this goal and should open avenues for further advances, particularly if combined with appropriate calibration systems or with freeze fracture techniques. A thorough discussion of quantitative aspects of immunocytochemistry is provided by Griffiths (1993).

As set out in the Introduction, the use of gold particles facilitates quantitation. Gold particles represent an "all or none signal," setting them apart from the less easily quantifiable reaction product of enzyme-based immunocytochemistry. The particles can be readily identified and counted in the electron microscope, and computer programs have been designed for automated acquisition and analysis of their distribution (Blackstad *et al.*, 1990; Haug *et al.*, 1994, 1996; Monteiro-Leal *et al.*, 2003; Ruud and Blackstad, 1999). In most cases, each gold particle deposit can be regarded as the result of an independent antigen–antibody reaction, permitting the use of simple statistics. Hence, one would predict a linear relationship between the gold particle density and the number of available antigen molecules (Ottersen, 1989b; also see Posthuma *et al.*, 1988).

The major obstacle to quantitation resides not in the counting and analysis of gold particles but in the nature of the underlying event: the antibody–antigen coupling. A *conditio sine qua non* for a meaningful quantitation of a sample of antigen molecules is that each molecule in the sample faces the same likelihood of encountering and binding to an antibody molecule. In practice, this requirement is difficult to fulfill. Preembedding procedures pose particular problems, as diffusion barriers imposed by membranes and other tissue constituents will bias the access of immunoreagents to the target molecules. This bias remains even with optimum permeabilization of the tissue in question. With the postembedding immunogold technique, the problem of diffusion constraints is eliminated, as the sample of target antigens is restricted to those molecules that are available at the cut surface of the section. Diffusion to the interior of the section is effectively hindered by the resin. Thus, an attractive feature of the postembedding approach is that all molecules in the sample are equally likely to be visualized by the immunocytochemical procedure.

The situation in practice is probably not as simple (Griffiths, 1993). Access to antibodies may be skewed by the surface relief of the section, and epitopes may be obscured by protein–protein interactions. Also, sterical hindrance between the rather bulky immunoreagents may reduce the probability of

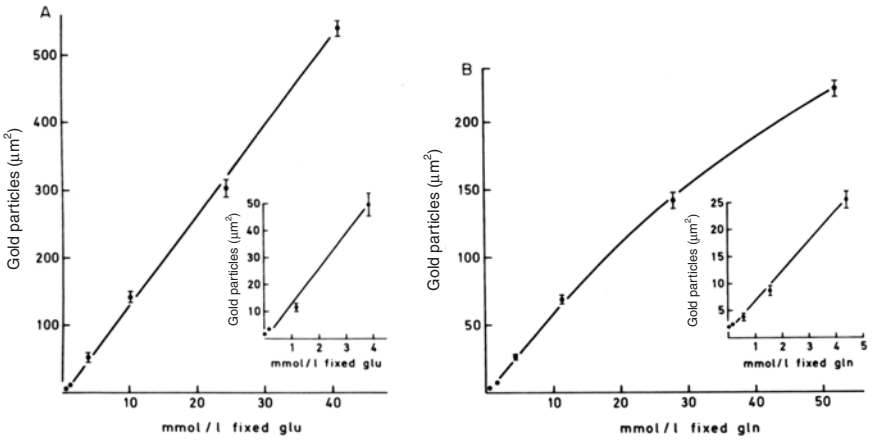

Figure 3.6. A calibration system tailor-made for postembedding immunogold cytochemistry (Ottersen, 1989b) demonstrates linear relationship between antigen concentration (mmol/l fixed glutamate in A; glutamine in B) and gold particle density (recorded over antigen-containing bodies such as those shown in Fig. 3.7). The linear relationship tends to break down at very high (biologically irrelevant) antigen concentrations (B). The lower ends of the plots are shown at larger scale in insets. The slopes and correlation coefficients for the two regression lines were 12.4 and 0.99 (glutamate, all data points included) and 5.4 and 1.00 (glutamine, estimated for data points shown in inset). (From Ottersen *et al.*, 1992.)

labeling at sites of very high antigen concentrations. This notwithstanding, by use of model antigens it has been shown that a linear relationship indeed can be obtained between antigen concentration and gold particle density.

We have used conjugated amino acids as model antigens (Ottersen, 1987, 1989b). Incorporation of radiolabeled amino acids allowed the concentration of antigen to be determined. Antigens in known concentrations were embedded in resin and sectioned for postembedding immunogold labeling and electron microscopy. For a series of different model antigens, it could be shown that the gold particle density was positively and linearly correlated with the calculated concentration of antigen molecules (Ottersen, 1989b; Ottersen *et al.*, 1992; Fig. 3.6). As predicted, in some cases the linearity was found to break down at very high antigen levels, probably as a result of steric hindrance.

The sections that were used to establish the correlation between the antigen concentration and the gold particle density could be incubated together with tissue sections and under exactly the same conditions as these. We thus had in our hands a calibration system that allowed us to determine the approximate concentration of antigen in different cells and organelles. This approach was used, inter alia, to assess the concentration of glutamate in nerve terminals, neuronal cell bodies, and astrocytes (Ottersen, 1989b; Ottersen *et al.*, 1992), and in organelles such as mitochondria and synaptic vesicles (Shupliakov *et al.*, 1992).

Aprerequisite for an adequate use of calibration curves is knowledge of the fraction of antigens that are retained in the tissue after fixation. In the

case of small molecules such as neurotransmitter amino acids, this is not a trivial problem, as substantial amounts may be lost from the tissue during the fixation procedure. With optimum fixation, using 1% glutaraldehyde or more, the retention of free amino acids exceeds 80%. This could be shown by equilibrating the tissue with tracer amounts of radiolabeled amino acids prior to fixation by immersion or perfusion (Storm-Mathisen and Ottersen, 1990).

When used in conjunction with appropriate model systems such as the one described above, postembedding immunocytochemistry permits an assessment of amino acid concentrations in cell compartments down to the level of synaptic vesicles and other organelles. In principle, this approach is applicable to all antigens that are available in pure form and that can be incorporated in calibration systems that are representative of the mode of antigen expression in vivo (see Griffiths, 1993, for a detailed discussion).

Plasma membrane proteins represent a more difficult case in regard to quantitation than small organic molecules or proteins that are distributed in the aqueous interior of the cell. For membrane proteins, a representative calibration system should be based on model membranes containing known concentrations of the protein in question. Ideally, the model membranes should have a composition similar to that of the membrane in which the protein is expressed in vivo. Obviously, these antigen-containing model membranes would have to be embedded and sectioned in parallel with the tissue and subjected to simultaneous immunoprocessing. It has proved difficult to develop model systems that meet all of these requirements. Unfortunately, therefore, postembedding immunogold cytochemistry of membrane proteins remains semiquantitative rather than quantitative.

To circumvent the difficulties entailed in developing a calibration system for membrane proteins, one may take advantage of quantitative immunoblotting and stereological data. Quantitative immunoblotting provides an estimate of the amount of a given protein per volume unit of tissue, whereas stereological analyses can be used to determine the total distribution surface for that protein (such as the total astrocytic surface in the case of a membrane protein that is restricted to astrocytes). In this way, one may calculate the average number of protein molecules per unit area of plasma membrane, as has been done for astroglial glutamate transporters (Lehre and Danbolt, 1998). This value can be correlated to the linear density of gold particles signaling the molecule in question. In principle, one ends up with a "correction factor" that can be used subsequently to translate gold particle densities into densities of target proteins.

Instead of calibrating the immunogold signal to biochemical data, one can relate the number of gold particles to functional parameters, such as the magnitude of synaptic currents in the case of postsynaptic receptors. Nusser *et al.* (1998) used this approach to assess the number of alpha-amino-3-hydroxy-5-methyl-4-isoxazole-propionic acid (AMPA) receptors at hippocampal synapses. One gold particle in postembedding-labeled methacrylate sections was found to correspond to 2.3 functional receptors, allowing estimates of synaptic receptor content.

As pointed out above, the major challenge in quantitation is to provide an accurate conversion factor between the number of gold particles and the number of tissue antigens. However, the analysis of particle distribution is not trivial, even if one refrains from assumptions regarding the underlying pattern of antigen distribution. Computer-based methods are indispensable if one embarks on large projects that involve sampling of several animals, blocks, sections, and images. In early studies in our laboratory, we digitized photographic prints by means of a digitizing table and counted particles with an electronic pen under control of the computer programs Morforel (Blackstad *et al.*, 1990) and Palirel (Ruud and Blackstad, 1999). Today, our main tool for quantifying immunogold labeling is IMGAP (IMmuno-Gold-Analysis-Program), created in our laboratory (Haug *et al.*, 1994, 1996). This program was developed in collaboration with SIS (Soft Imaging Systems Gmbh, Münster, Germany) as an extension to their product analySIS. IMGAP permits automated acquisition of gold particles, taking advantage of their high electron density and defined sizes. Appendix II describes the typical workflow when using IMGAP. The web site http://www.med.uio.no/imb/stat/immunogold/index.html is a service for methods and programs for statistical analysis of immunogold data.

Simplified methods are applicable when the biological problem at hand is limited to that of comparing immunogold labeling patterns in the same sets of compartments across different cells (Mayhew *et al.*, 2004). In this situation, no information may be required about compartment size or membrane length.

Rapid assessments of gold particle distributions can be obtained by use of simple stereological methods. One example from our own laboratory is described in Landsend *et al.* (1997), based on preparations such as that shown in Fig. 3.5. Using a stereological approach, Lucocq *et al.* (2004) claimed that counting 100–200 particles on each of two grids may be sufficient to produce a rough estimate of the gold particle distribution over as many as 10–16 different compartments. This should be kept in mind when designing an immunogold analysis so as to avoid excessive and pointless counting of gold particles.

Finally, it should be emphasized that the freeze fracture–immunogold technique represents a quite different approach to quantitation, holding great promise for the future (for review, see Rash *et al.*, 2004). Accurate quantitation should be feasible for any protein that can be immunodetected in freeze fracture replicas and that has structural features that set it apart from other IMPs in the same membrane domain. The limited ability to differentiate between different IMPs, based on their morphological appearance, remains a problem in this regard.

Closely related to the issue of quantitation is the term *labeling efficiency*. This term refers to the ratio between the number of gold particles and the number of antigen molecules that is available for immunolabeling. Labeling efficiency depends on many factors that have been addressed in studies of cryosections (e.g., Griffiths and Hoppeler, 1986). As pointed out

by Griffiths (1993), it is probable that the labeling efficiency is always below 100% in postembedding-labeled sections. A rough estimate of the labeling efficiency can be obtained by analysis of membrane domains that contain known densities of the target proteins (derived, e.g., from correlative freeze fracture analyses). In a postembedding immunogold analysis of AMPA receptors in hippocampal synapses, it was shown that the number of gold particles increased by one particle per ~15-nm increment in the length of synaptic profile (Takumi *et al.*, 1999). Based on the known size of AMPA receptors and conservative estimates of their spacing, these data suggest that there is a close to 1:1 stoichiometry between gold particles and AMPA receptors at the section surface, given optimum experimental conditions.

Factors that affect labeling efficiency include quality of antibody, fixation procedure, embedding medium, and incubation parameters (Griffiths, 1993; Matsubara *et al.*, 1996). Several of these factors are addressed below, in the discussion of our "standard" postembedding immunogold procedure. Optimization of the postembedding immunogold procedure for a given antigen is very much a question of obtaining maximum labeling efficiency. High labeling efficiency is of critical importance in postembedding immunogold analyses because of the restricted sample of accessible epitopes, and becomes a decisive factor in analyses of membrane proteins that are expressed at low densities. Indeed, the choice of immunocytochemical procedure (pre- or postembedding) should always be based on available information on the prevalence of the antigen at hand.

IV. CONTROLS

The need for appropriate controls in immunocytochemistry can hardly be overemphasized. As a discussion of the general principles for assessing antibody selectivity is outside the scope of the present chapter, we will restrict ourselves to procedures that are specific for postembedding immunogold cytochemistry.

Testing of selectivity must be done in conditions that are representative of the conditions of the immunocytochemical procedure. This is because the conformation of the epitope and the nature of the antibody–epitope interaction may be influenced by a number of factors, such as the choice of fixative and resin and the selection of incubation parameters. In other words, showing that the antibody identifies a single band at the appropriate molecular weight in immunoblots cannot be taken to imply that the antibody provides selective labeling in the postembedding mode. Immunocytochemistry and antibody testing should be performed in parallel and under identical conditions.

This criterion can be met in the case of small molecules such as amino acids and larger antigens that are available in pure form (Davanger *et al.*, 1994; Ottersen, 1987). The target antigen and structurally related molecules can be embedded in resin, sectioned, and immunoincubated together with

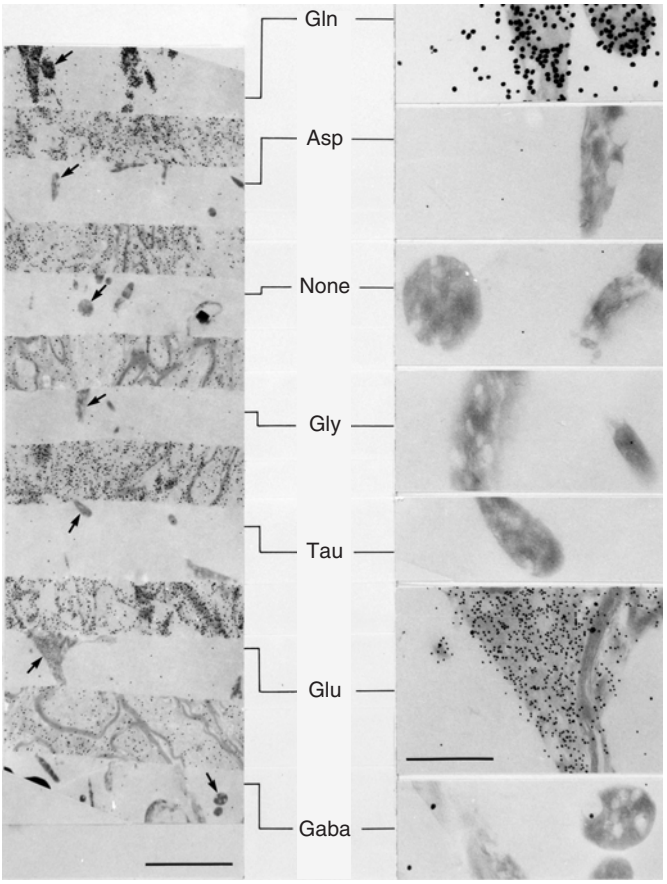

Figure 3.7. Test system designed to monitor antibody selectivity under the conditions of the immunocytochemical procedure. The target antigens and structurally homologous molecules were embedded in resin and incorporated in a test sandwich with alternating brain sections used as spacers. Ultrathin cross sections of this sandwich were incubated together with the tissue sections. The test antigens appear as dense bodies. Bodies identified by arrows are enlarged in the right part of the figure. In this case, the test antigens were prepared by coupling glutamate (Glu), glutamine (Gln), and structurally related amino acids (standard abbreviations) to brain macromolecules in the presence of glutaraldehyde. The test section shown here and the accompanying tissue section (Fig. 3.8) were double labeled for glutamate (15-nm particles) and glutamine (30-nm particles) using a modification of the procedure of Wang and Larsson (1985) (see Ottersen *et al.*, 1992, for details). Quantitative analysis of this test section (Ottersen *et al.*, 1992) confirmed that the antisera react selectively with the target antigen in the actual conditions used for fixation, embedding, and immunoincubation. The quantitative analysis also showed that the present double-labeling procedure (using two antibodies from the same species) distinguishes between the two antigens with negligible interference. (From Ottersen *et al.*, 1992)

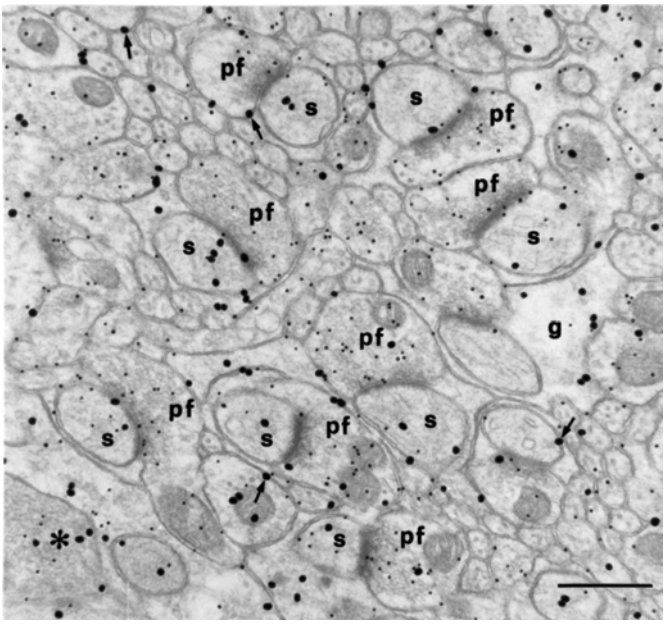

Figure 3.8. Section from the molecular layer of rat cerebellum incubated together with the test section shown in Fig. 3.7. The high selectivity obtained in the test section should be representative of the selectivity in the tissue section. Small gold particles signaling fixed glutamate are enriched in parallel fiber terminals (pf), whereas large gold particles signaling glutamine mainly decorate glial processes (g) and Purkinje cell dendritic spines (s). Asterisk, possible climbing fiber; arrows, intercellular clefts. Scale bar: 0.4 μm. (From Ottersen *et al.*, 1992.)

the tissue sections. This approach provides a direct and reliable validation of antibody selectivity. In the example shown here (Figs. 3.7 and 3.8), it could be documented that antibodies to glutamate and glutamine distinguish between the respective amino acids, despite their close structural similarity. The degree of cross-reactivity could be determined quantitatively (Ottersen *et al.*, 1992; Fig. 3.7). It is important that the test antigens are exposed to the same fixative as the target antigen in the tissue. Specifically, in the case of amino acids, these must be conjugated to brain proteins by glutaraldehyde before embedding and testing (Ottersen, 1987; Storm-Mathisen *et al.*, 1983). In this way, the test antigens will mimic the complexes that are formed in the tissue during perfusion fixation, when the fixative (glutaraldehyde) cross-links free amino acids to brain macromolecules.

Positive controls such as that discussed above document the ability of the antibody to differentiate between structurally similar epitopes. However, negative controls are required to ascertain that the immunogold signal represents antibody binding to the target antigen rather than unspecific labeling. Such controls are particularly important when the target antigen is believed to reside in nuclei, mitochondria, postsynaptic densities, or other sites that promote unspecific binding due to high protein concentrations. The most powerful negative control is provided by the availability of animals

with a selective knockout of the gene encoding the target protein. Pending knockout animals, transfection experiments (comparing cells with and without the antigen in question) constitute a useful substitute. One must not put too much emphasis on standard absorption experiments (involving neutralization of the primary antibody by application of an excess of the immunizing peptide), as these do not differentiate between specific and unspecific binding of the antibody clone in question (for a comprehensive discussion of specificity controls, see Holmseth et al., 2005).

V. APPLICATIONS

It is outside the scope of the present chapter to provide a comprehensive discussion of the range of biological problems to which the postembedding immunogold technique can be successfully applied. In our own laboratory, we have found this technique to be particularly useful for the following purposes:

1. Demonstration of protein colocalization by use of double labeling with two different-sized gold particles (Fig. 3.9; also see Fig. 3.15). This application takes advantage of the discrete sizes of gold particles and the fact that double labeling can be successfully performed, with minimum cross-reactivity (Fig. 3.7), even when the two primary antisera are derived from the same species (Ottersen *et al.*, 1992; Wang and Larsson, 1985).
2. Demonstration of receptors and amino acid transmitter (e.g., glutamate) in the same synapses by use of double labeling (Matsubara *et al.*, 1996; Takumi *et al.*, 1999; Fig. 3.10). This procedure requires the use of glutaraldehyde in the fixative to retain the amino acid in question (see section "Postembedding Procedures").
3. Combination of postembedding labeling and anterograde tracing to identify transmitters and receptors in specific fiber projections (Ji *et al.*, 1991; Ragnarson *et al.*, 1998, 2003; Rinvik and Ottersen, 1993; Fig. 3.11).
4. Investigation of disease mechanisms at high resolution. Examples: analysis of glutamate redistribution in experimental stroke to explore the mechanisms of excitotoxic cell death (Torp *et al.*, 1993), and analysis of the mechanisms of β-amyloid generation in Alzheimer's disease and relevant animal models (Torp *et al.*, 2000, 2003; Fig. 3.12).
5. Phenotypic analyses of transgene animals to demonstrate changes in subcellular expression of neuronal or glial proteins (Amiry-Moghaddam *et al.*, 2003a,b; Amiry-Moghaddam and Ottersen, 2003; Kohr *et al.*, 2003; Neely *et al.*, 2001; Rossi *et al.*, 2002).

VI. POSTEMBEDDING PROCEDURES

The hallmark of postembedding immunocytochemistry is that the tissue is embedded in a resin prior to the immunocytochemical procedure. As most

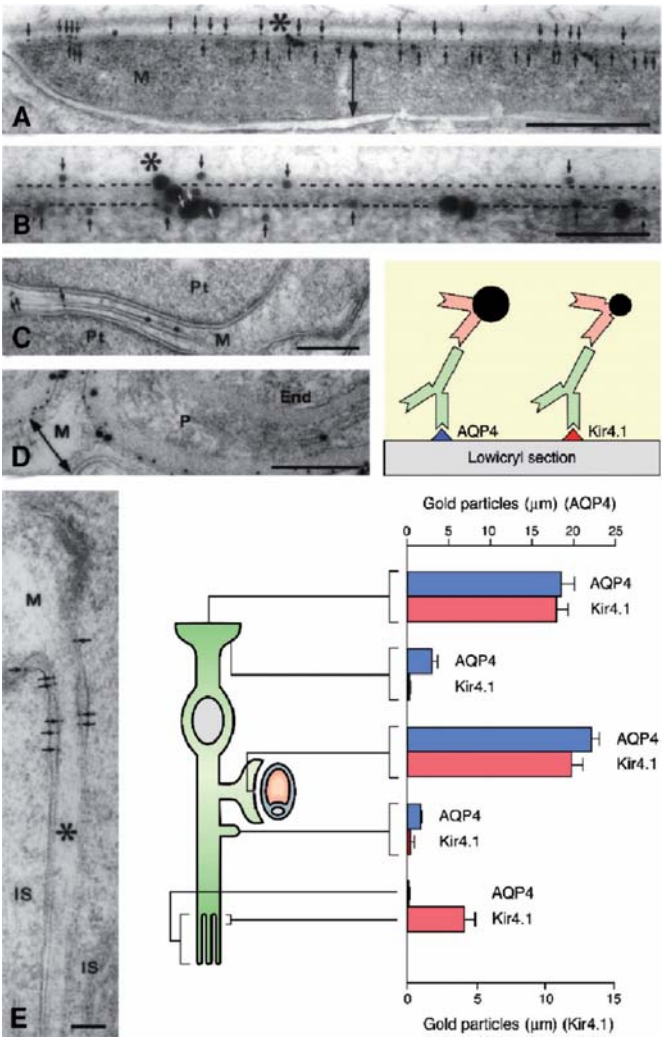

Figure 3.9. Semiquantitative analysis of subcellular expression patterns of two protein antigens. Double immunogold labeling of Kir4.1 (10-nm particles) and AQP4 (20-nm particles) in vitreal (A, B), perisynaptic (C), and perivascular (D) Müller cell (M) membranes. (A, B) The M end foot (M) is selectively labeled at its vitreal aspect (both aspects indicated by double arrow). The vitreal plasma membrane (between dashed lines in B) is obliquely cut, allowing labeling at the two sides of the section to be distinguished. Small arrows indicate Kir4.1 labeling. Asterisks indicate corresponding points at the vitreal surface (part of A is enlarged in B). (C) Weak Kir4.1 (arrows) and AQP4 labeling is found in the thin Müller cell processes (M) that surround photoreceptor terminals (Pt). (D) Perivascular end feet (M) shows a polarized distribution of gold particles (double arrow, compare with A). End, endothelial cell; P, pericyte. (E) Kir4.1 immunolabeling of an M microvillus (asterisk). The gold particles (arrows) are restricted to its basal part which is devoid of large particles signaling AQP4. IS, inner segment of photoreceptors. Scale bars: 0.5 μm (A); 0.1 μm (B, E); 0.25 μm (C, D). The graph shows linear densities of gold particles in different membrane domains of M. (Modified from Nagelhus *et al.*, 1999.)

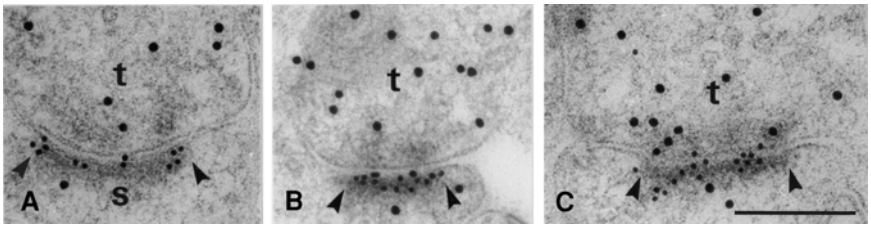

Figure 3.10. Double immunogold labeling of transmitter and receptor in synapses from stratum radiatum of rat hippocampus. Large gold particles signal fixed glutamate, and small particles signal NMDA receptors. Arrowheads indicate extent of postsynaptic densities. t, nerve terminal. Scale bar: 200 nm. (From Takumi *et al.*, 1999.)

resins are hydrophobic, the tissue water has to be replaced by an organic solvent before the infiltration step. Thus, the sequence of steps is as follows:

1. Fixation
2. Dehydration
3. Embedding (infiltration and polymerization of resin)
4. Sectioning
5. Immunoincubation
6. Electron microscopic analysis of sections

Each of the steps above can be performed in many different ways. In fact, there are about as many recipes as there are laboratories in the field. The reasons why there is such a plethora of procedures are that each laboratory has a unique set of needs and that the protocol has to be tailored to the antigen at hand. The latter point cannot be overemphasized: for each new target antigen, one must be prepared to modify the procedure for optimum results. This is why postembedding immunocytochemistry is oftentimes challenging and sometimes frustrating—and very rewarding when it works.

Any researcher who enters into the field of postembedding immunocytochemistry will soon realize that many antibodies will never work, regardless of fixation, embedding, and incubation conditions. Unfortunately, the performance of a given antibody in postembedding immunogold analyses cannot be predicted from its performance in immunoblots or immunofluorescence. An element of "trial and error" is inevitable.

Appendix I provides an outline of the protocol that is currently being used in our own laboratory for the initial screening of a novel protein antigen. Optimization of this protocol for a given protein may require substantial modifications, as emphasized below.

We will first provide a general discussion of the major steps of the procedure, starting with tissue fixation.

A. Fixation

As for immunocytochemistry in general, the choice of fixative is a tradeoff between the need to preserve tissue ultrastructure and the need to

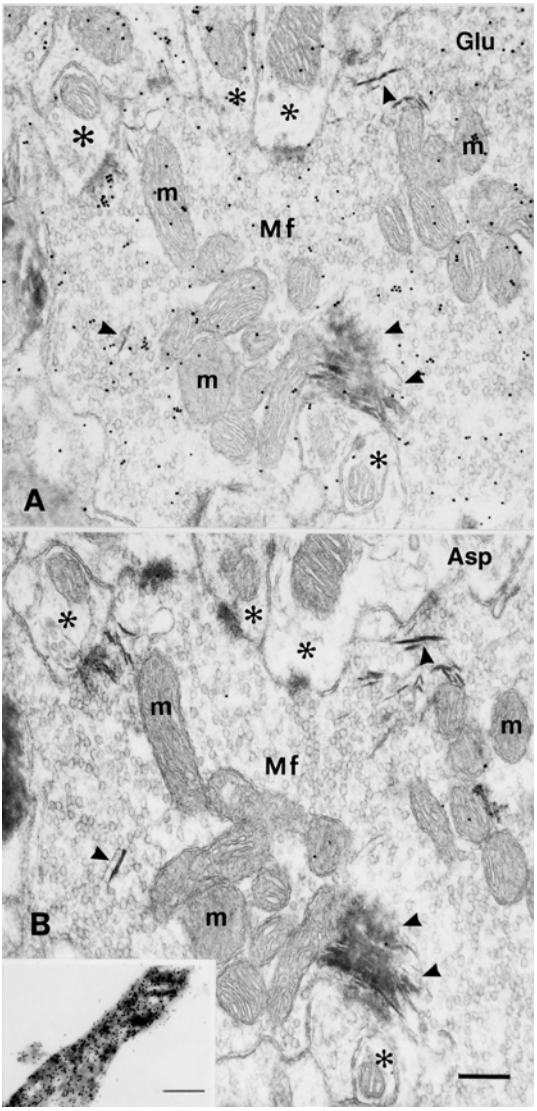

Figure 3.11. Combination of anterograde labeling and postembedding immunogold cytochemistry. Spinocerebellar terminals were identified by anterograde transport of horseradish peroxidase conjugated to wheat germ agglutinin (HRP-WGA). The HRP reaction product is indicated by arrowheads. The anterogradely labeled mossy fiber terminal (Mf) is immunopositive for glutamate (A) but immunonegative for aspartate (B; section adjacent to that in A). The absence of aspartate immunolabeling is not a false-negative result as aspartate-containing model conjugates, incubated together with the tissue section, showed strong immunogold labeling (inset in B). m, mitochondria; asterisks, granule cell dendritic digits. Scale bars: 0.2 μm (A, B); 0.6 μm (inset). (From Ji *et al.*, 1991.)

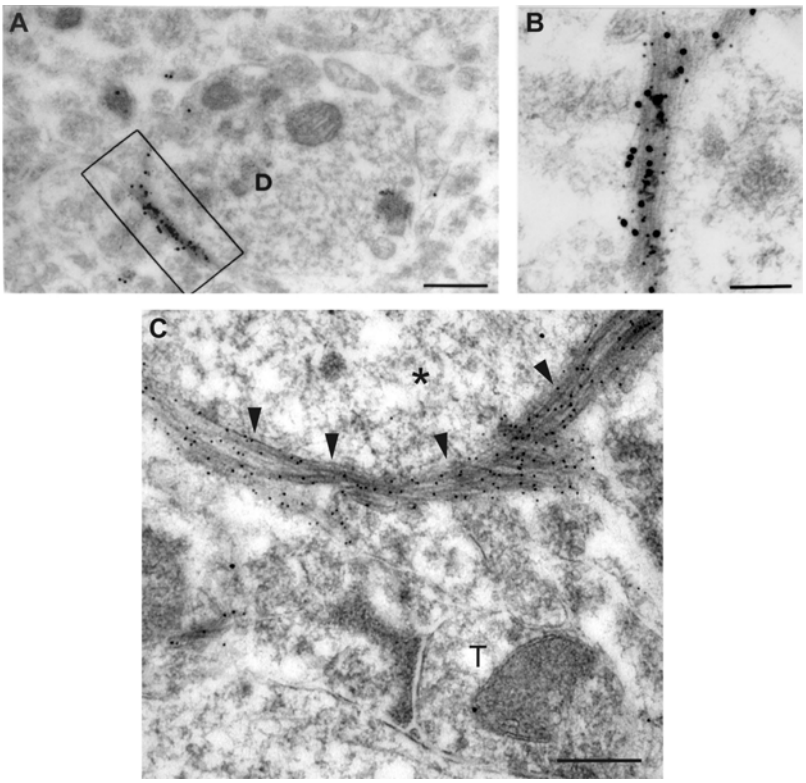

Figure 3.12. (A, B) Plasma membrane domains show coexpression of presenilin 1 (PS1) and amyloid (Aβ 42). Double immunogold labeling reveals colocalization of Aβ (large particles) and PS1 (small particles) in a discrete patch of neuronal plasma membrane in somatosensory cortex of an aged canine. Framed area in A is enlarged in B. D, dendrite. Scale bars: 0.3 μm (A); 0.2 μm (B). (From Torp *et al.*, 2000.) (C) Postembedding immunogold labeling of amyloid plaque in the hippocampus of a transgenic mouse model of Alzheimer's disease (3XTg-AD). Arrowheads point to extracellular deposit of amyloid. Intracellular compartments (asterisk) are devoid of gold particles. Antibody to Aβ 42. T, terminal. Scale bar: 0.4 μm (R. Torp, 2006).

preserve the antigen in a form that can be recognized by the specific antibodies. Strong fixatives, with a high concentration of glutaraldehyde, provide the best ultrastructure, whereas weak fixatives, with little or no glutaraldehyde, provide optimum preservation of antigenicity and hence the strongest immunocytochemical signal. The concentration of glutaraldehyde is more critical than the concentration of formaldehyde, as glutaraldehyde is bivalent (it has two reactive aldehyde groups). As such, glutaraldehyde is a very efficient cross-linker. Cross-linking of tissue macromolecules affords good ultrastructure but may severely distort or mask the target epitopes. In our hands, it is impossible to predict the amount of glutaraldehyde that a given antigen will tolerate. For some membrane proteins, glutaraldehyde

concentrations as high as 1% have proved to be compatible with a strong immunogold signal. Our standard protocol (i.e., the protocol used for the first screening of a novel protein target) is based on the use of 0.1% glutaraldehyde in combination with 4% formaldehyde.

Visualization of neuroactive amino acids (such as glutamate, γ-amino butyric acid (GABA), and glycine) represents a special case (Ottersen, 1987; Somogyi *et al.*, 1986; Somogyi and Hodgson, 1985), as these small molecules are lost from the tissue unless they are irreversibly cross-linked to tissue macromolecules (Dale *et al.*, 1986; Ottersen, 1989a; Storm-Mathisen *et al.*, 1983). Thus, immunocytochemical analysis of amino acids and other small molecules with free amino groups (including glutathione; Hjelle *et al.*, 1994) requires the inclusion of significant amounts of glutaraldehyde. We have shown that 1% glutaraldehyde is sufficient to retain the major proportion of free amino acids. Concentrations as low as 0.1% may yield a good signal, permitting double labeling of a transmitter amino acid and its respective receptor (e.g., visualization of presynaptic glutamate and postsynaptic AMPA receptors in the same synapses; Takumi *et al.*, 1999). However, the lower the glutaraldehyde concentration, the greater the risk for a skewed retention of amino acids across the different cell compartments.

B. Dehydration and Embedding

For protein antigens in the central nervous system, the combination of freeze substitution and embedding in methacrylate resins has become very popular (Griffiths, 1993; Humbel and Schwarz, 1989; Matsubara *et al.*, 1996; Nusser *et al.*, 1998; van Lookeren Campagne *et al.*, 1991). This is also the standard procedure in our own laboratory. This combination of techniques is designed to preserve the original conformation of the protein antigen. For analyses of brain, we prefer to fix the tissue before freezing rather than at later stages in the process.

The first step is to cryoprotect the fixed tissue specimen by immersion in glycerol or sucrose. The specimen is then frozen, usually by plunging it into liquid propane. Freezing must be obtained as quickly as possible, in order to avoid loss of ultrastructure due to the formation of ice crystals (Griffiths, 1993). Liquid propane has a higher temperature than liquid helium but is considered superior to the latter since it allows a faster dissipation of heat from the tissue specimen. Obviously, the size of the specimen must be restricted in order to permit rapid freezing. In practice, we usually refrain from exceeding 1 mm in any dimension.

Once frozen, the tissue specimen is transferred from the cryofixation unit to a cryosubstitution unit. This unit supports three sequential processes:

1. Substitution of methanol for ice
2. Substitution of resin for methanol (i.e., infiltration)
3. Polymerization of resin by ultraviolet (UV) light

The overall effect of processing the tissue in the cryosubstitution unit is to replace ice with polymerized resin. The substitutions occur at very low temperatures and are therefore very slow, requiring several days to complete. In the cryosubstitution unit, contrast is conferred by exposure of the tissue to uranyl acetate, which has affinity for biological membranes. Uranyl acetate takes the place of osmium tetroxide, commonly used to provide contrast when the tissue is embedded in epoxy resins. Osmium tetroxide absorbs light and can be used only in low concentrations in combination with UV polymerization.

The freeze substitution procedure outlined above differs significantly from the classical procedure for dehydration and embedding. The classical procedure is based on postfixation of the tissue in osmium tetroxide, followed by dehydration, infiltration in an epoxy resin, and polymerization. These steps typically take place at room temperature (RT), except for the polymerization process which is run at 60°C, depending on the type of epoxy resin.

Although procedures based on the use of epoxy resins can be modified for visualization of proteins in the postembedding mode (Phend *et al.*, 1995; Salio *et al.*, 2005), the freeze substitution procedure is usually considered as superior. Our own experience with a number of protein antigens is that the latter procedure provides a much stronger immunosignal and higher signal-to-noise ratio than do procedures based on epoxy resins. Several factors have been proposed to explain why freeze substitution provides such an advantage:

1. All steps, including polymerization, are run at low temperatures, reducing the risk of protein denaturation.
2. Methacrylate resins can accommodate a certain amount of water, possibly allowing for a partial preservation of the proteins' hydration shells.
3. The polymerization of methacrylate resins does not engage the proteins to the same extent as does the polymerization of epoxy resins, reducing the risk of distorting or masking the target epitopes.
4. Due in part to their unique polymerization features, methacrylate resins provide for a more pronounced surface relief than do epoxy resins. In other words, proteins at the cut surface tend to stick out of the plane of section rather than being bisected.

In sum, these mechanisms may help retain the original conformation of the target protein and preserve its antigenicity (Griffiths, 1993). The freeze substitution procedure is also well suited for nonproteinaceous antigens such as neuroactive amino acids, allowing for double labeling analyses (Fig. 3.10; also see Matsubara *et al.*, 1996).

A range of methacrylate resins is available. The different resins differ primarily by their ability to accommodate water and by their fluidity. In principle, given the fact that proteins are normally expressed in an aqueous environment, high hydrophilicity should translate into a better preservation

of protein conformation. For glutamate receptors and a number of plasma membrane transporters in the central nervous system, we have observed rather minor differences between different methacrylate resins when it comes to the strength of the immunosignal. Our standard procedure is based on the use of Lowicryl HM20, which is one of the more hydrophobic methacrylates. Very hydrophilic methacrylates may be difficult to work with due to inadvertent swelling of the sections once they are exposed to water.

C. Immunoincubation

Postembedding immunogold labeling of ultrathin sections usually comprises the following steps:

1. "Etching" of section to increase the availability of epitopes at the section surface
2. Blocking of unspecific binding of antibodies
3. Application of primary antibody
4. Application of secondary IgG, Fab, or protein A coupled to colloidal gold

The goal is to end up with a distribution of gold particles that truly reflects the distribution of target epitopes, given the constraints imposed by the size of the antibody bridge (Fig. 3.1). To minimize variability, the sections and grids to be analyzed should be included in the same batch for simultaneous incubation.

Appendix I shows the immunoincubation procedure that is in current use as our standard laboratory protocol. The standard protocol has been modified over the years (Chaudhry *et al.*, 1995; Hjelle *et al.*, 1994; Nagelhus *et al.*, 2005) and has been influenced strongly by protocols published from other laboratories (e.g., Nusser *et al.*, 1998; van Lookeren Campagne *et al.*, 1991). In fact, as is the case for immunocytochemical procedures in general, postembedding procedures evolve continuously as parameters are tested out and as resins and reagents improve.

The outcome of an immunoincubation depends on the combined effect of a number of different steps. In fact, the enormous number of permutations that can be obtained by combining variations of the different steps precludes a bona fide scientific approach to optimization of the procedure. This is unfortunate, as several steps in current use may have been carried over from other experimental settings, which may or may not be representative of the procedure in question.

For the purpose of the present chapter, we have performed a systematic variation of key parameters to assess their relative importance for the strength of the immunogold signal (measured as the number of gold particles per micrometer membrane following immunogold visualization of the water channel protein AQP4). As shown in Fig. 3.13, the choice of secondary IgG/colloidal gold conjugate profoundly affects the signal strength

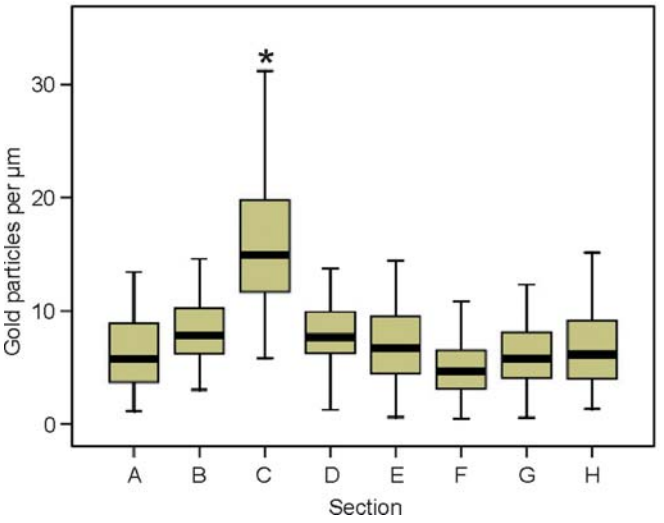

Figure 3.13. Quantitative assessment of how incubation parameters influence labeling efficiency. Preparations similar to that showed in Fig. 3.3A, postembedding labeled with an antibody to AQP4, were subjected to automated analysis of gold particle density by the procedure outlined in Appendix II. The labeling intensity (particles per micrometer perivascular membrane) depended on the combination of incubation parameters (A–H). Reference conditions (A) were identical to those of the "standard" protocol in Appendix I. These were sodium ethanolate (etching), 2% HSA (blocking), 0.04 M NaCl (in buffer), 0.1% Triton (T), 15-nm gold particles. B–H differed from A in the following ways. B: no sodium ethanolate; C: 10-nm gold particles; D: no HSA; E: 0.01% T; F: 0.2% milk powder in lieu of HSA; G: 0.12 M NaCl; H: identical to G, but analyzed by a different person (to check for consistency). Sixty membrane segments were analyzed for each combination of parameters.

(compare A and C). Secondary IgG coupled to 10-nm particles leads to a higher linear density of gold particles than does a secondary IgG coupled to 15-nm particles. This effect relates primarily to the size of gold particle (rather than differences between the two IgGs) as qualitative analyses of a wider range of particle sizes point to a negative correlation between gold particle size and signal strength. Steric hindrance may be one of the several factors that underlie this effect.

A logical extension of the latter observations would be to minimize the gold particle size to maximize the labeling efficiency. Gold particles that are less than 5 nm in diameter are not easily discerned in postembedding-labeled sections, calling for silver enhancement if smaller particles are used. Application of nanogold particles in combination with silver enhancement indeed leads to a significant increase in gold particle density, as shown in postembedding immunogold labeling of glutamate receptors (Matsubara *et al.*, 1996; also see Fig. 3.17). However, such preparations pose difficulties in quantitative analyses: The silver-enhanced particles are less uniform than gold particles in regard to size and shape, and their stoichiometric relationship to the target antigens is less well defined.

Another parameter that may affect signal strength is the concentration of NaCl in the buffer of the primary and secondary antibody steps. It is well known that antibody–antigen binding depends on a number of different forces, including ion bonds between oppositely charged residues in the antibody and antigen molecules. Thus, ions in the buffer (primarily Na^+ and Cl^- ions) would be expected to compete with antigen–antibody binding. This prediction was borne out in our postembedding analysis of AMPA glutamate receptors (Matsubara *et al.*, 1996) and led us to lower the NaCl concentration of the buffer (typically to one third of that of physiological saline) whenever an increased signal strength was wanted. In the case of AQP4, the effect of reducing the salt concentration is negligible (compare A with G in Fig. 3.13), underlining the fact that the significance of the different parameters depends on the nature of the target antigen.

Blocking of unspecific binding is an essential step in postembedding immunocytochemistry as in immunocytochemistry in general. Unspecific binding may be caused by a wide range of mechanisms. Obviously, when aldehydes are used for fixation, there is a risk that reactive aldehyde groups remain in the tissue and that these groups attach the immunoreagents to the section. For this reason, we always include glycine and TRIS in the first blocking buffer. Both of these molecules have free amino groups that would bind to and neutralize any free aldehyde groups at the section surface.

We also regularly use human serum albumin (HSA) to prevent unspecific binding of IgG. Fortunately, the inclusion of up to 2% of HSA does not cause any inadvertent reduction in the strength of the specific signal (compare A with D in Fig. 3.13). Milk powder is also in common use as a blocking agent, but our experience is that it is difficult to adjust its concentration so as to provide a reduction of background labeling without affecting the specific signal. In fact, in our quantitative analysis of AQP4 immunolabeling we recorded a reduction in gold particle density when exchanging 2% HSA with 0.2% milk powder (compare A with F in Fig. 3.13). The use of well-defined blocking agents (such as HSA) is encouraged for the purpose of standardization and reproducibility. Very low background labeling can be obtained with adequate blocking procedures (cf. Figs. 3.5 and 3.14).

The etching step is probably the most problematic step to justify in the postembedding immunogold protocol. As alluded to above, the purported aim of this step is to improve access to the target epitopes. However, it is not clear to what extent the commonly used etching procedure (a short immersion in sodium ethanolate; see Appendix I) removes resin and unmasks surface epitopes. In fact, our quantitative analysis of AQP4 suggests that there is no gain in immunogold signal by including this step (compare A with B in Fig. 3.13). Leaving out the etching steps also allows for excellent labeling of glutamate receptors and intracellular enzymes (Figs. 3.15 and 3.16). It should be emphazised that the comparison in Fig. 3.13 was done in the presence of Triton. Triton might help unmask epitopes at the section surface (by dissolving lipids) and could easily obscure any positive effect of the etching procedure. Pending a systematic analysis of the interaction

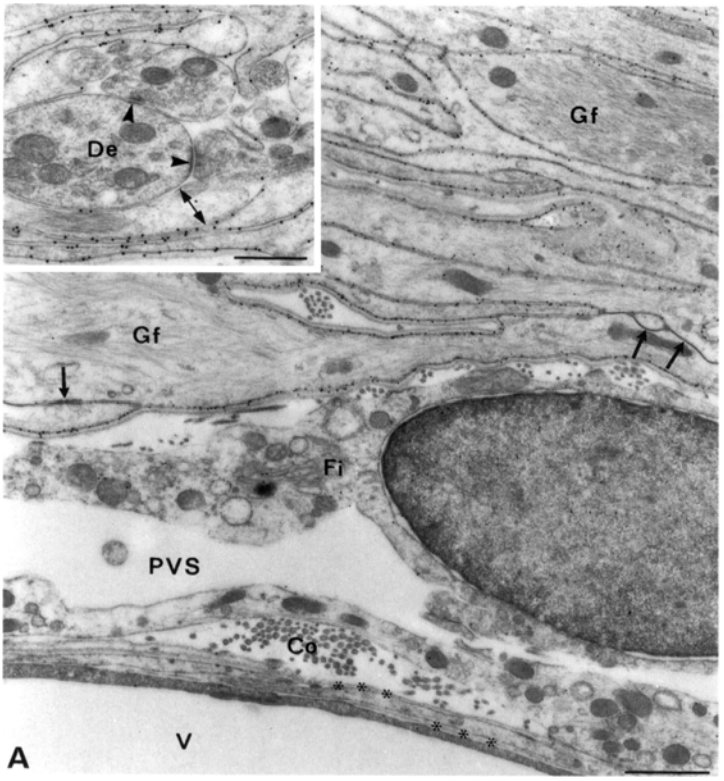

Figure 3.14. High signal-to-noise ratio afforded by optimization of postembedding immunogold procedure. Gold particles signal expression of AQP4 in the subfornical organ of rat. Immunogold particles identify AQP4 along the entire glial lamellae except at the membrane domains engaged in gap or adhaerens type junctions (arrows) or contacting neuronal elements (double-headed arrow in inset). The vessel (V) and associated basal laminae (asterisks) are devoid of AQP4 immunolabeling. Co, collagen; Fi, fibroblast; Gf, glial filaments; PVS, perivascular space. Inset: unlabeled synapses (arrowheads) sandwiched between glial lamellae. The adjacent glial processes are polarized with respect to AQP4 expression (double-headed arrow). De, dendrite. Scale bars: 1 μm. (Micrographs by E. Nagelhus taken From Nielsen *et al.*, 1997).

between etching and Triton application, the possibility exists that the etching step represents an unjustified adoption to methacrylate resins of a step that has been shown to work well with epoxy resins. In the absence of a proven effect, the etching step should be omitted as it significantly detracts from the quality of the ultrastructure. Again it should be recalled that the effect of etching (or lack thereof) may not be the same for all antigens.

The above discussion amply documents that immunocytochemistry is still an art and not a science. Quantitative analyses such as that shown in Fig. 3.13 can be used to monitor the effect of changing an individual parameter, but the magnitude of effect, if any, may depend on the other parameters and on the nature of the antigen. The take-home message is that the postembedding immunogold procedure must be tailored to one's needs and to

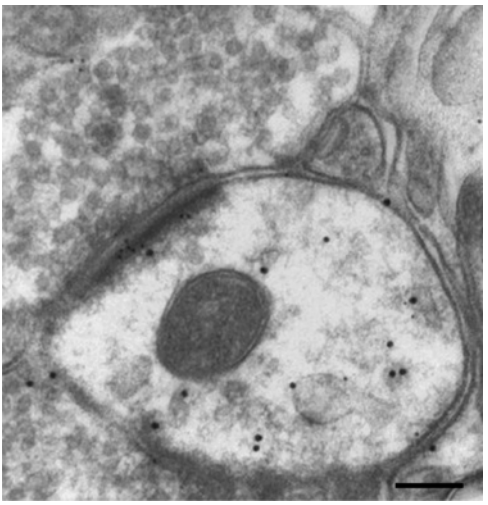

Figure 3.15. Omission of etching (conditions as in Fig. 3.13B but with 0.01% Triton) is compatible with high labeling efficiency. The sections were first immunolabeled with an antibody against tyrosine hydroxylase (20-nm gold particles), and after 1 h in formaldehyde vapor at 80°C (procedure of Wang and Larsson, 1985) the sections were immunolabeled with antibodies recognizing NMDA receptor subunits A and B (10-nm gold particles). From ventral tegmental area of rat. (Micrograph by E. Rinvik, 2006.)

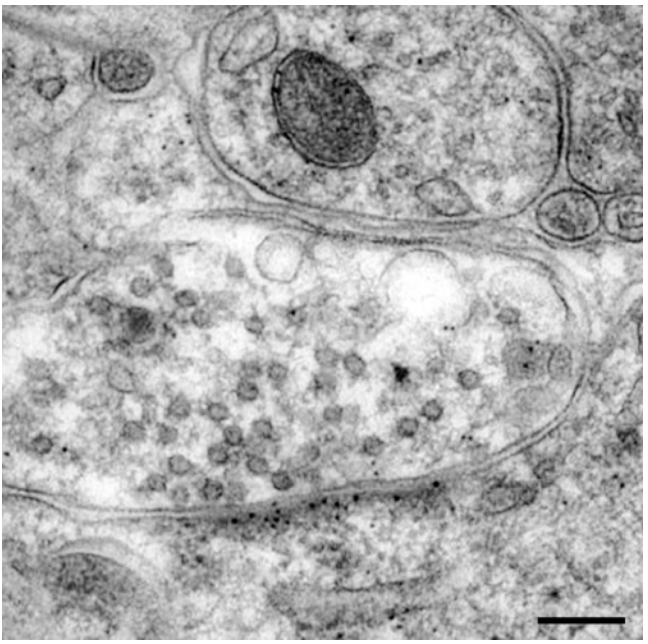

Figure 3.16. Omission of etching allows high labeling efficiency and good ultrastructural preservation (compare with Fig. 3.10). Same procedure as in Fig. 3.15, but single labeling with antibodies to AMPA receptor subunits 2 and 3. From ventral tegmental area of rat. (Micrograph by E. Rinvik, 2006.)

one's targets. This is often a major challenge but a challenge well worth taking because of the wealth of information that can be gained when an immunogold experiment succeeds.

APPENDIX I: A POSTEMBEDDING IMMUNOGOLD PROCEDURE FOR MEMBRANE PROTEINS

This procedure permits double labeling with antibodies to glutamate, GABA, or other neuroactive amino acids (Takumi *et al.*, 1999).

A. Tissue Preparation

Note. Steps 5–10 are carried out in a computer-controlled cryosubstitution unit.

1. Anesthetize the animal. Perfuse transcardially with 2% dextran (MW 70,000) in 0.1 M sodium phosphate buffer (PB; pH 7.4, 15 s at RT) followed by a mixture of glutaraldehyde (0.1%) and formaldehyde (4%; freshly depolymerized from paraformaldehyde) in the same buffer (for rats, 50 ml/min for 20 min at RT).
2. Leave the brain in situ overnight (4°C).
3. Isolate tissue specimens from brain, cryoprotect by immersion in increased concentrations of glycerol (10, 20, and 30% in PB), 0.5 h for each concentration (RT), and then overnight in 30% (4°C).
4. Place the tissue on the specimen pin and plunge into propane cooled to −170°C by LN2 in a cryofixation unit (Reichert KF80, Vienna, Austria).
5. Transfer the specimens to 1.5% uranyl acetate dissolved in anhydrous methanol (- 90°C) in a cryosubstitution unit (AFS; Reichert). After 30 h, raise the temperature stepwise (4°C increment per hour) from −90 to −45°C.
6. Wash the samples three times with anhydrous methanol.
7. Infiltrate with Lowicryl HM 20 resin (Polysciences, Inc., Warrington, PA 18976. Cat# 15924) at −45°C.
   (a) Lowicryl/methanol: 1:1, 2 h
   (b) Lowicryl/methanol: 2:1, 2 h
   (c) Pure Lowicryl: 2 h
   (d) Pure Lowicryl: overnight
8. Change to freshly prepared Lowicryl and move the Reichert capsules with the specimens to the Lowicryl-filled gelatin capsules in the G-chamber.
9. Transfer the capsules to a container filled with ethanol.
10. Polymerize with UV light. Start at −45°C (24 h), and then increase temperature to 0°C (increment 5°C/h). Complete the polymerization at 0°C (35 h).

11. Prepare ultrathin sections at 80- to 100-nm thickness and mount on nickel rids or gold-coated grids for immunogold cytochemistry.

B. Immunoincubation

1. Etch sections in saturated sodium ethanolate (can be omitted; cf. text) for 2–5 s.
2. Rinse well in distilled water for 3× short and 1 × 10 min. Let dry and check that the sections are in place.
3. Place grids into a grid support plate (Leica cat. no. 705698) and immerse in 50 mM glycine in TBST (Tris-buffered saline with 0.1% Triton X-100 or 0.01% Triton; cfr. text) for 10 min.
4. Preincubate in TBST containing 2% HSA for 10 min.
5. Incubate in primary antibody diluted in TBST containing 2% HSA for 2 h, overnight in RT.
6. Rinse in TBST for 3× short, 1 × 10 min and 3× short, 1 × 10 min.
7. Preincubate in TBST containing 2% HSA for 10 min.
8. Incubate in secondary antibody (IgGs coupled to colloidal gold particles). Dilute as recommended from the company and with 2% HSA and 0.05% polyethyleneglycol (PEG) for 1 h.
9. Rinse briefly 6× in distilled water, dry sections.
10. Incubate in 5% uranyl acetate in 40% ethanol for 90 s.
11. Rinse briefly 3× in distilled water, dry sections.
12. Incubate in lead citrate for 90 s.
13. Rinse briefly 3× in distilled water, dry sections.

C. Solutions

Sodium ethanolate: Add 100 g NaOH in 700 ml 100% ethanol.

TBST: 100 ml 0.05 M Tris buffer, pH 7.4 (pH adjusted with HCl); 900 ml ultrafiltered (UF) water containing 0.9% NaCl; 1 g Triton X-100.

Lead citrate: Dissolve 1.33 g lead nitrate and 1.76 g sodium citrate in 30 ml UF water. Stir for 30 min. Add 8 ml 1 M NaOH and fill up to 50 ml with UF water. Aliquot in 10 ml syringes and store protected from light in refrigerator.

D. Protocol for Postembedding Immunogold Labeling Using Ultrasmall Gold Particles Coupled to Fab Fragments (Secondary Antibodies) and Silver Intensification (Fig. 3.17)

1. Rinse grids in MilliQ filtered (18.2 MΩ) water for 1 min
2. TBST containing 0.1% sodium borohydride and 50 mM glycine
3. Blocking buffer 10 min
4. Primary antiserum 2 h or overnight

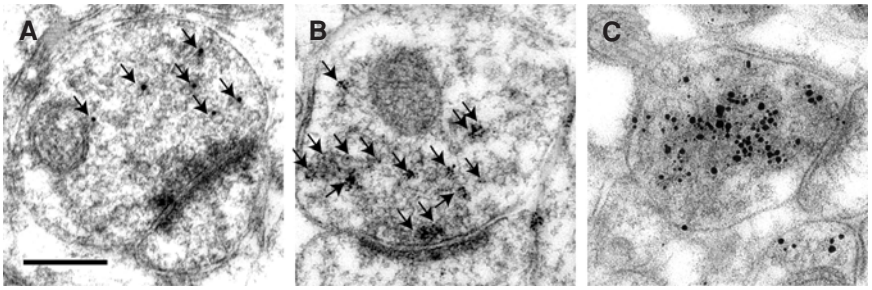

Figure 3.17. Silver enhancement provides increased labeling intensity of synaptic vesicle proteins. (A) Postembedding labeling of SV2 using 10-nm colloidal gold coupled to the secondary antibody. (B) Same as in A, but with 1.4-nm gold particles ("Nanogold") coupled to a secondary Fab fragment and followed by silver enhancement. (C) Same as in B, but with antibody to synaptophysin. Note clusters of small silver deposits in B, and larger silver deposits due to longer reaction time in C. Silver intensification gives silver deposits of varying sizes, prohibiting double-labeling experiments. (Micrographs by S. Davanger, unpublished data.)

5. TBST 1 min
6. Blocking buffer 3× 1 min
7. Nanogold Fab 1:40 in blocking buffer containing PEG 2000
8. Phosphate-buffered saline (PBS) 3× 1 min
9. Glutaraldehyde 1% in PBS 3 min
10. Water 2 × 1 min
11. HQ silver Nanoprobes (N.B. safelight!)
12. Water 3 × 5 min
13. Dry sections
14. Uranyl acetate 2% 40 min
15. Water 4 × 1 min
16. Dry sections
17. Lead citrate 0.3% 3 min
18. Water 4 × 1 min
19. Dry sections

TBST (1000 ml): 100 ml 0.05 M Tris, pH 7.4; 900 ml MilliQ water with 0.9% NaCl; 1 g Triton X-100.

Blocking Buffer (1500 µl): 2% (30 µl) normal goat serum; 1% (125 µl of 12% stock solution) bovine serum albumin; 0.5% (7.5 µl) Tween 20; TBST 1337.5 µl.

APPENDIX II: COUNTING IMMUNOPARTICLES BY DIGITAL IMAGE ANALYSIS

Computer support may substantially reduce the time to completion of large projects, as illustrated by the IMGAP software referred to in the text. The latter combines interactive and automated procedures for image

storage and retrieval, particle counting over organelles and membranes, calculation of areal and linear densities, and conversion of the final data set to a statistics program for further analyses. The following workflow does not distinguish between native analySIS functions and in-house extensions.

1. "Define" an "IMGAP project": Create a project folder with section folders to hold all images, ancillary information, and results. Define project-wide pick lists of Field types (see point 6 for a definition of Field in this context) and Object types ("objects" are transected spines, postsynaptic densities, etc.). Select measurements (native to analySIS or defined in IMGAP) to be automatically carried out on each object.
2. Choose the electron optic magnification that provides the best compromise between digital resolution, required field of view, and the size of the digital image file. Since lossy compression methods should be avoided, projects with many large images may run into several gigabytes, not a problem with today's storage facilities.
3. Capture TIFF images with any suitable camera and software and subsequently import them into IMGAP, or capture images with analySIS while keeping IMGAP active for online access to the project-wide pick list of image labels and possibly other services.
4. Freehand draw transected organelles as Regions of Interest (ROIs), and membranes as curves, attaching a type label to each such graphic object.
5. After background smoothing and global intensity thresholding, detect and classify particles in up to three size classes.
6. Inspect the result and revise if necessary, by changing parameters for automated procedures or by interactively deleting, adding, or splitting particles. In particular, although particle detection is partly automated, its quality depends 100% on the operator.

   Each ROI, curve, and particle is now uniquely identified and geometrically described by analySIS. Together with analySIS, IMGAP ensures that they are automatically stored with the corresponding image in "revisable format" and automatically displayed in the overlay whenever an image is reloaded. In IMGAP, an image with associated ROIs, curves, and particles, and other associated information, is termed a field (i.e., "field of view").
7. Automatically aggregate and export particle measurements (data on each particle in the project) to SPSS. Use to create transverse histograms for each "type" of membrane and for "quality control" of the detected particles (cf. point 6).
8. Automatically calculate areal density of particles per ROI, aggregate over the project, and export to SPSS.
9. Prior to calculating linear densities along membranes, set a distance filter to eliminate particles too far off the curve.
10. Export ROI and curve measurements for further graphical and statistical analyses.

11. In the SPSS data set, each object (ROI, curve, or particle) has one line and each measurement or other characteristic one column. Check the data set for errors as recommended in standard statistics textbooks and software manuals. Each measurement is traceable to the underlying image, and so errors may be diagnosed and corrected.
12. For images in need of corrections, repeat steps 4–6. Then go on to steps 7 and 8.
13. Further analyses are performed in SPSS or other software (the SPSS formats are compatible with a range of other statistics software, but more manual calculations may also be required). Also see web site http://www.med.uio.no/imb/stat/immunogold/index.html.

An important source of error in the above procedures should be noted. Due to simplistic particle-detection and quality-control algorithms, *small* falsely positive particles may easily go unnoticed unless the operator is alert to this possibility in step 6 and has been duly trained to optimize the parameters for steps 2, 3, and 5. Increased intensity resolution (14 rather than 12 bits) may improve on this, as emphasized by Monteiro-Leal *et al.* (2003), and in addition, the algorithms for particle detection and quality control should be improved.

Limited digital resolution and operator error during interactive drawing (step 4) may add error, presumably random. Obviously, both the automatically detected particles and the interactively drawn curves will be more accurate with increasing resolution. Compared to the "basic uncertainty zone" which surrounds immunogold attached via primary and secondary antibodies, the present inaccuracy may be thought insignificant. However, when planning histograms with 1-nm bins, select the electron optic magnification with a view to the resulting object pixel dimensions (the size of a pixel projected to the specimen). To illustrate this, our MegaView III camera (trademark of Soft Imaging Systems) has a nominal *xy* resolution just above 1280 × 1024 pixels. Mounted on our Tecnai 12 it renders a specimen area of 2.1 μm × 1.6 μm, with an object pixel size of 1.5 nm at a nominal electron optical magnification of 49,000×. (As an aside, with these parameters, 10-nm gold particles come out with diameters around 4–6 pixels and the particle detection algorithm still works satisfactorily.)

While a digital resolution of 1280 × 1024 pixels is small in relation to digital cameras in this year's (2005) consumer market, the price–performance ratio on cameras for electron microscopy remains two orders of magnitude higher. If you need higher digital resolution, automated image montage, in analySIS represented by the MIA module, may be an alternative, although in our hands its success rate is often less than 100%.

Acknowledgments. Support is acknowledged from the Norwegian Research Council, the Nordic Council (the centre of excellence programme in molecular medicine), and EU (projects QLG3-CT-2001-02089 and LSHM-CT-2005-005320).

REFERENCES

Amiry-Moghaddam, M., Otsuka, T., Hurn, P. D., Traystman, R. J., Haug, F. M., Froehner, S. C., Adams, M. E., Neely, J. D., Agre, P, Ottersen, O. P., and Bhardwaj, A., 2003a, An alpha-syntrophin-dependent pool of AQP4 in astroglial end-feet confers bidirectional water flow between blood and brain, *Proc. Natl. Acad. Sci. USA* **100**(4):2106–2111.

Amiry-Moghaddam, M., and Ottersen, O. P., 2003, The molecular basis for water transport in brain, *Nat. Rev. Neurosci.* **4**(12):991–1001.

Amiry-Moghaddam, M., Williamson, A., Palomba, M., Eid, T., de Lanerolle, N. C., Nagelhus, E. A., Adams, M. E., Froehner, S. C., Agre, P., and Ottersen, O. P., 2003b, Delayed K^+ clearance associated with aquaporin-4 mislocalization: phenotypic defects in brains of alpha-syntrophin-null mice, *Proc. Natl. Acad. Sci. USA* **100**(23):13615–13620.

Blackstad, T. W., Karagulle, T., and Ottersen, O. P., 1990, MORFOREL, a computer program for two-dimensional analysis of micrographs of biological specimens, with emphasis on immunogold preparations, *Comput. Biol. Med.* **20**(1):15–34.

Chaudhry, F. A., Lehre, K. P., van Lookeren Campagne, M., Ottersen, O. P., Danbolt, N. C., and Storm-Mathisen, J., 1995, Glutamate transporters in glial plasma membranes: highly differentiated localizations revealed by quantitative ultrastructural immunocytochemistry, *Neuron* **15**(3):711–720.

Dale, N., Ottersen, O. P., Roberts, A., and Storm-Mathisen, J., 1986, Inhibitory neurones of a motor pattern generator in *Xenopus* revealed by antibodies to glycine, *Nature (Lond)* **324:**255–257.

Davanger, S., Hjelle, O. P., Babaie, E., Larsson, L. I., Hougaard, D., Storm-Mathisen, J., and Ottersen, O. P., 1994, Colocalization of gamma-aminobutyrate and gastrin in the rat antrum: an immunocytochemical and in situ hybridization study, *Gastroenterology* **107**(1):137–148.

Didier, A., Carleton, A., Bjaalie, J. G., Vincent, J. D., Ottersen, O. P., Storm-Mathisen, J., and Lledo, P. M., 2001, A dendrodendritic reciprocal synapse provides a recurrent excitatory connection in the olfactory bulb, *Proc. Natl. Acad. Sci. USA* **98:**6441–6446.

Faulk, W. P., and Taylor, G. M., 1971, An immunocolloid method for the electron microscope, *Immunochemistry* **11:**1081–1083.

Fujimoto, K., 1995, Freeze-fracture replica electron microscopy combined with SDS digestion for cytochemical labeling of integral membrane proteins. Application to the immunogold labeling of intercellular junctional complexes, *J. Cell Sci.* **108:**3443–3449.

Griffiths, G., 1993, *Fine Structure Immunocytochemistry*, Berlin: Springer-Verlag, p. 459.

Griffiths, G., and Hoppeler, H., 1986, Quantitation in immunocytochemistry: correlation of immunogold labeling to absolute number of membrane antigens, *J. Histochem. Cytochem.* **34**(11):1389–1398.

Hagiwara, A., Fukazawa, Y., Deguchi-Tawarada, M., Ohtsuka, T., and Shigemoto, R., 2005, Differential distribution of release-related proteins in the hippocampal CA3 area as revealed by freeze-fracture replica labeling, *J. Comp. Neurol.* **489**(2): 195–216.

Haug, F. M., Desai, V. D., Nergaard, P. O., Laake, J., and Ottersen, O. P., 1994, Particle-counting in immunogold labelled ultrathin sections by transmission electron microscopy and image analysis, *Anal. Cell. Pathol.* **6:**197.

Haug, F. M. S., Desai, V., Nergaard, P. O., and Ottersen, O. P., 1996, Quantifying immunogold labelled neurotransmitters and receptors by image analysis, *Soc. Neurosci. Abstr.* **22**(1):581.

Hjelle, O. P., Chaudhry, F. A., and Ottersen, O. P., 1994, Antisera to glutathione: characterization and immunocytochemical application to the rat cerebellum, *Eur. J. Neurosci.* **6**(5):793–804.

Holmseth, S., Dehnes, Y., Bjornsen, L. P., Boulland, J. L., Furness, D. N., Bergles, D., and Danbolt, N. C., 2005, Specificity of antibodies: unexpected cross-reactivity of antibodies direct against the excitatory amino acid transporter 3(EAAT3), *Neuroscience* **136**: 649–660.

Hu, H., Shao, L. R., Chavoshy, S., Gu, N., Trieb, M., Behrens, R., Laake, P., Pongs, O., Knaus, H. G., Ottersen, O. P., and Storm, J. F., 2001, Presynaptic Ca^{2+}-activated K^+ channels in

glutamatergic hippocampal terminals and their role in spike repolarization and regulation of transmitter release, *J. Neurosci.* **21**(24):9585–9597.

Humbel, B. M., and Schwartz, H., 1989, Freeze-substitution for immunochemistry, In: Verkleij, A. J., and Leunissen, J. L. M. (eds.), *Immunogold Labelling in Cell Biology*, Boca Raton, FL: CRC Press, pp. 115–134.

Ji, Z. Q., Aas, J. E., Laake, J., Walberg, F., and Ottersen, O. P., 1991, An electron microscopic, immunogold analysis of glutamate and glutamine in terminals of rat spinocerebellar fibers, *J. Comp. Neurol.* **307**(2):296–310.

Kohr, G., Jensen, V., Koester, H. J., Mihaljevic, A. L., Utvik, J. K., Kvello, A., Ottersen, O. P., Seeburg, P. H., Sprengel, R., and Hvalby, O., 2003, Intracellular domains of NMDA receptor subtypes are determinants for long-term potentiation induction, *J. Neurosci.* **23**(34):10791–10799.

Landsend, A. S., Amiry-Moghaddam, M., Matsubara, A., Bergersen, L., Usami, S., Wenthold, R. J., and Ottersen, O. P., 1997, Differential localization of delta glutamate receptors in the rat cerebellum: coexpression with AMPA receptors in parallel fiber-spine synapses and absence from climbing fiber-spine synapses, *J. Neurosci.* **17**(2):834–842.

Lehre, K. P., and Danbolt, N. C., 1998, The number of glutamate transporter subtype molecules at glutamatergic synapses: chemical and stereological quantification in young adult rat brain, *J. Neurosci.* **18**(21):8751–8757.

Lucocq, J. M., Habermann, A., Watt, S., Backer, J. M., Mayhew, T. M., and Griffiths, G., 2004, A rapid method for assessing the distribution of gold labeling on thin sections, *J. Histochem. Cytochem.* **52**(8):991–1000.

Matsubara, A., Laake, J. H., Davanger, S., Usami, S., and Ottersen, O. P., 1996, Organization of AMPA receptor subunits at a glutamate synapse: a quantitative immunogold analysis of hair cell synapses in the rat organ of Corti, *J. Neurosci.* **16**(14):4457–4467.

Maunsbach, A. B., and Afzelius, B. A., 1999, *Biomedical Electron Microscopy: Illustrated Methods and Interpretations*, San Diego: Academic Press, 548 p.

Mayhew, T. M., Griffiths, G., and Lucocq, J. M., 2004, Applications of an efficient method for comparing immunogold labelling patterns in the same sets of compartments in different groups of cells, *Histochem. Cell Biol.* **122**(2):171–177.

Monteiro-Leal, L. H., Troster, H., Campanati, L., Spring, H. F., and Trendelenburg, M., 2003, Gold finder: a computer method for fast automatic double gold labeling detection, counting, and color overlay in electron microscopic images, *J. Struct. Biol.* **141**(3): 228–239.

Nagelhus, E. A., Horio, Y., Inanobe, A., Fujita, A., Haug, F. M., Nielsen, S., Kurachi, Y., and Ottersen, O. P., 1999, Immunogold evidence suggests that coupling of K^+ siphoning and water transport in rat retinal Muller cells is mediated by a coenrichment of Kir4.1 and AQP4 in specific membrane domains, *Glia* **26**(1):47–54.

Nagelhus, E. A., Mathiisen, T. M., Bateman, A. C., Haug, F. M., Ottersen, O. P., Grubb, J. H., Waheed, A., and Sly, W. S., 2005, Carbonic anhydrase XIV is enriched in specific membrane domains of retinal pigment epithelium, Muller cells, and astrocytes, *Proc. Natl. Acad. Sci. USA* **102**(22):8031–8035.

Nagelhus, E. A., Mathiisen, T. M., and Ottersen, O. P., 2004, Aquaporin-4 in the central nervous system: cellular and subcellular distribution and coexpression with KIR4.1, *Neuroscience* **129**(4):905–913.

Nagelhus, E. A., Veruki, M. L., Torp, R., Haug, F. M., Laake, J. H., Nielsen, S., Agre, P., and Ottersen, O. P., 1998, Aquaporin-4 water channel protein in the rat retina and optic nerve: polarized expression in Muller cells and fibrous astrocytes, *J. Neurosci.* **18**(7): 2506–2519.

Neely, J. D., Amiry-Moghaddam, M., Ottersen, O. P., Froehner, S. C., Agre, P., and Adams, M. E., 2001, Syntrophin-dependent expression and localization of aquaporin-4 water channel protein, *Proc. Natl. Acad. Sci. USA* **98**(24):14108–14113.

Nielsen, S., Nagelhus, E. A., Amiry-Moghaddam, M., Bourque, C., Agre, P., and Ottersen, O. P., 1997, Specialized membrane domains for water transport in glial cells: high-resolution immunogold cytochemistry of aquaporin-4 in rat brain, *J. Neurosci.* **17**(1):171–180.

Nusser, Z., Lujan, R., Laube, G., Roberts, J. D., Molnar, E., and Somogyi, P., 1998, Cell type and pathway dependence of synaptic AMPA receptor number and variability in the hippocampus, *Neuron* **21**(3):545–559.

Ottersen, O. P., 1987, Postembedding light- and electron microscopic immunocytochemistry of amino acids: description of a new model system allowing identical conditions for specificity testing and tissue processing, *Exp. Brain Res.* **69**(1):167–174.

Ottersen, O. P., 1989a, Quantitative electron microscopic immunocytochemistry of amino acids, *Anat. Embryol.* **180:**1–15.

Ottersen, O. P., 1989b, Postembedding immunogold labelling of fixed glutamate: an electron microscopic analysis of the relationship between gold particle density and antigen concentration, *J. Chem. Neuroanat.* **2**(1):57–66.

Ottersen, O. P., Zhang, N., and Walberg, F., 1992, Metabolic compartmentation of glutamate and glutamine: morphological evidence obtained by quantitative immunocytochemistry in rat cerebellum, *Neuroscience* **46:**519–534.

Panzanelli, P., Homanics, G. E., Ottersen, O. P., Fritschy, J. M., and Sassoe-Pognetto, M., 2004, Pre- and postsynaptic GABA receptors at reciprocal dendrodendritic synapses in the olfactory bulb, *Eur. J. Neurosci.* **20**(11):2945–2952.

Phend, K. D., Rustioni, A., and Weinberg, R. J., 1995, An osmium-free method of epon embedment that preserves both ultrastructure and antigenicity for post-embedding immunocytochemistry, *J. Histochem. Cytochem.* **43**(3):283–292.

Posthuma, G., Slot, J. W., Veenendaal, T., and Geuze, H. J., 1988, Immunogold determination of amylase concentrations in pancreatic subcellular compartments, *Eur. J. Cell Biol.* **46**(2):327–335.

Ragnarson, B., Ornung, G., Grant, G., Ottersen, O. P., and Ulfhake, B., 2003, Glutamate and AMPA receptor immunoreactivity in Ia synapses with motoneurons and neurons of the central cervical nucleus, *Exp. Brain Res.* **149**(4):447–457.

Ragnarson, B., Ornung, G., Ottersen, O. P., Grant, G., and Ulfhake, B., 1998, Ultrastructural detection of neuronally transported choleragenoid by postembedding immunocytochemistry in freeze-substituted Lowicryl HM20 embedded tissue, *J. Neurosci. Methods* **80**(2):129–136.

Rash, J. E., Davidson, K. G., Yasumura, T., and Furman, C. S., 2004, Freeze-fracture and immunogold analysis of aquaporin-4 (AQP4) square arrays, with models of AQP4 lattice assembly, *Neuroscience* **129**(4):915–934.

Rinvik, E., and Ottersen, O. P., 1993, Terminals of subthalamonigral fibres are enriched with glutamate-like immunoreactivity: an electron microscopic, immunogold analysis in the cat, *J. Chem. Neuroanat.* **6**(1):19–30.

Rossi, P., Sola, E., Taglietti, V., Borchardt, T., Steigerwald, F., Utvik, J. K, Ottersen, O. P., Kohr, G., and D'Angelo, E., 2002, NMDA receptor 2 (NR2) C-terminal control of NR open probability regulates synaptic transmission and plasticity at a cerebellar synapse, *J. Neurosci.* **22**(22):9687–9697.

Roth, J., 1996, The silver anniversary of gold: 25 years of the colloidal gold marker system for immunocytochemistry and histochemistry, *Histochem. Cell Biol.* **106**(1):1–8.

Ruud, H. K., and Blackstad, T. W., 1999, PALIREL, a computer program for analyzing particle-to-membrane relations, with emphasis on electron micrographs of immunocytochemical preparations and gold labeled molecules, *Comput. Biomed. Res.* **32**(2):93–122.

Salio, C., Lossi, L., Ferrini, F., Merighi, A., 2005, Ultrastructural evidence for a pre- and postsynaptic localization of full length trkB receptors in substantia gelatinosa (lamina II) of rat and mouse spinal cord, *Eur. J. Neurosci.* **22**(8): 1951–1966.

Shupliakov, O., Brodin, L., Cullheim, S., Ottersen, O. P., and Storm-Mathisen, J., 1992, Immunogold quantification of glutamate in two types of excitatory synapse with different firing patterns, *J. Neurosci.* **12**(10):3789–3803.

Somogyi, P., Halasy, K., Somogyi, J., Storm-Mathisen, J., and Ottersen, O. P., 1986, Quantification of immunogold labelling reveals enrichment of glutamate in mossy and parallel fibre terminals in cat cerebellum, *Neuroscience* **19**(4):1045–1050.

Somogyi, P., and Hodgson, A. J., 1985, Antisera to gamma-aminobutyric acid: III. Demonstration of GABA in Golgi-impregnated neurons and in conventional electron microscopic sections of cat striate cortex, *J. Histochem. Cytochem.* **33**(3):249–257.

Storm-Mathisen, J., Leknes, A. K., Bore, A. T., Vaaland, J. L., Edminson, P., Haug, F.-M. S., and Ottersen, O. P., 1983, First visualization of glutamate and GABA in neurones by immunocytochemistry, *Nature* **301:**517–520.

Storm-Mathisen, J., and Ottersen, O. P., 1990, Antibodies and fixatives for the immunocytochemical localization of glycine, In: Ottersen, O. P., and Storm-Mathisen, J. (eds.), *Glycine Neurotransmission*, Chichester: John Wiley & Sons, pp. 281–301.

Takumi, Y., Ramirez-Leon, V., Laake, P., Rinvik, E., and Ottersen, O. P., 1999, Different modes of expression of AMPA and NMDA receptors in hippocampal synapses, *Nat. Neurosci.* **2**(7):618–624.

Torp, R., Arvin, B., Le Peillet, E., Chapman, A. G., Ottersen, O. P., and Meldrum, B. S., 1993, Effect of ischemia and reperfusion on the extra- and intracellular distribution of glutamate, glutamine, aspartate, and GABA in the rat hippocampus, with a note on the effect of the sodium channel blocker BW1003C87, *Exp. Brain Res.* **96:**365–376.

Torp, R., Head, E., Milgram, N. W., Hahn, F., Ottersen, O. P., and Cotman, C. W., 2000, Ultrastructural evidence of fibrillar beta-amyloid associated with neuronal membranes in behaviorally characterized aged dog brains, *Neuroscience* **96:**495–506.

Torp, R., Ottersen, O. P., Cotman, C. W., and Head, E., 2003, Identification of neuronal plasma membrane microdomains that colocalize beta-amyloid and presenilin: implications for beta-amyloid precursor protein processing, *Neuroscience* **120**(2):291–300.

Valtschanoff, J. G., and Weinberg, R. J., 2001, Laminar organization of the NMDA receptor complex within the postsynaptic density, *J. Neurosci.* **21**(4):1211–1217.

van den Pol, A. N., 1989, Neuronal imaging with colloidal gold, *J. Microsc.* **155**(1):27–59.

van Lookeren Campagne, M., Oestreicher, A. B., van der Krift, T. P., Gispen, W. H., and Verkleij, A. J., 1991, Freeze-substitution and Lowicryl HM20 embedding of fixed rat brain: suitability for immunogold ultrastructural localization of neural antigens, *J. Histochem. Cytochem.* **39**(9):1267–1279.

Wang, B. L., and Larsson, L. I., 1985, Simultaneous demonstration of multiple antigens by indirect immunofluorescence or immunogold staining. Novel light and electron microscopical double and triple staining method employing primary antibodies from the same species, *Histochemistry* **83**(1):47–56.